

DISSECTING LUNAR EJECTA RADII AROUND COLD SPOT CRATERS. Tiffany Gao¹ and Aleksandra J. Sokołowska^{1,2}. ¹Brown University, Providence RI USA. (tiffany_gao@brown.edu) ²Imperial College London, London, UK.

Introduction: Impact craters on the Moon provide critical insights into subsurface properties and impact dynamics. Ejecta blankets, in particular, serve as indicators of subsurface composition, with rocky ejecta signifying consolidated layers and fine-grained ejecta suggesting unconsolidated materials [1]. Simulations of impact cratering [2] demonstrate that ejecta spatial distributions can vary based on subsurface rheology, highlighting the potential of scaled ejecta radius ($R_{\text{ejecta}} / R_{\text{crater}}$; [7]) as a new diagnostic tool. Detailed measurements of this quantity around young, well-preserved craters on the Moon are needed to evaluate their potential for constraining numerical models.

Cold spot craters have been identified as some of the Moon's youngest craters [5]. The freshness of the ejecta as well as the high level of detail that can be resolved in their morphology in LROC NAC images [8] make them ideal for studying ejecta characteristics (Fig. 1).

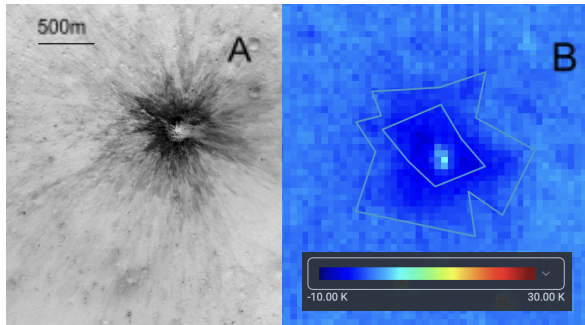


Fig. 1. An example of a cold spot crater shown in (B) Diviner H-Parameter data [9] where dark blue is low thermal inertia and light blue is higher (M1224603815RC). The colormap in A is inverted.

In this study, we analyze the ejecta of cold spot craters on the Moon. We focus on the general variability in scaled ejecta radii and their relationship with rock abundance which signifies difference in subsurface rheology.

Methodology:

We selected 50 cold spot craters from the existing database [10] for detailed analysis based on four primary factors: (1) size, (2) rock abundance, (3) the incidence angle of available LROC NAC images, and (4) geographic distribution.

Our study focuses on craters with diameters <700 m. Craters are also divided into four bins based on rock abundance: low ($H_{\text{Rock}} < 0.02$), moderate ($H_{\text{Rock}} 0.02–0.05$), high ($H_{\text{Rock}} 0.05–0.06$), and very high ($H_{\text{Rock}} > 0.07$). Whenever possible we also prioritized images with lower incidence angles as we found those to emphasize better the specifics of ejecta morphology.

To probe diverse subsurface compositions and terrains, we also ensured that craters span a wide range of latitudes and longitudes thereby capturing geological variability across basaltic mare regions and anorthositic highlands (Fig. 2).

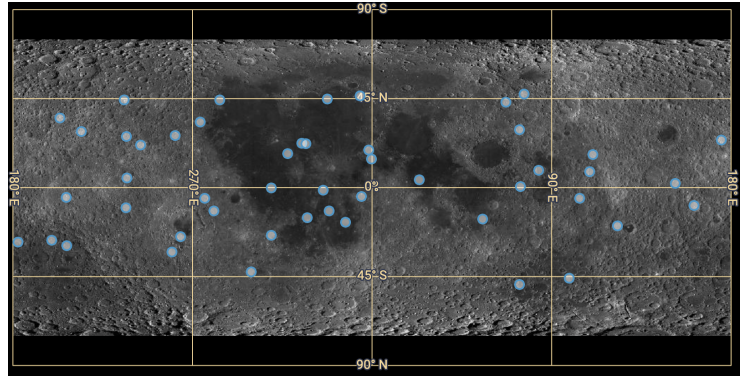
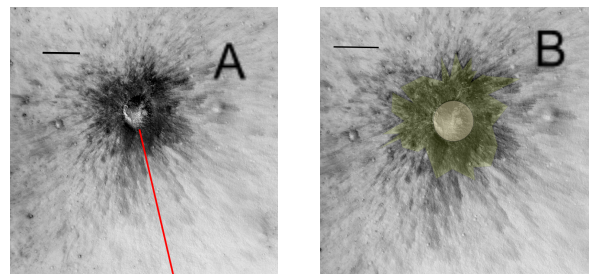


Fig. 2. Locations of the 50 cold spot craters selected for analysis (mapped in LROC Quickmap tool [8]).

We mapped ejecta blankets with QGIS [6] in LROC NAC images [8]. We found that inverting colormaps enhances the visibility of ejecta boundaries with respect to the background surface. In such inverted images, darker pixels in the center represent thicker ejecta than lighter pixels at the outer edges of the blanket. (Fig. 3A).

Ejecta blankets are typically divided into two components: continuous ejecta, which extend 2–3 crater radii ($2-3 R_{\text{cr}}$) from the center, and discontinuous ejecta, which extend beyond 3 radii [3-4]. Continuous ejecta blankets are characterized by the presence of relatively continuous debris on a planetary surface, while discontinuous ejecta exhibit patchy morphology in both radial and azimuthal directions.

Following this convention, we divided crater ejecta into similar distinct components. However, a closer inspection of radial transects of pixel intensity generated with the QGIS Profile Tool plugin (Fig. 3A,F) revealed several distinct features throughout the ejecta (drops in pixel intensity, see Fig. 3B-E), which led to our new classification scheme: continuous ejecta, and up to three discontinuous ejecta levels. This scheme allows us to study how to compare ejecta radii across a variety of targets and surfaces in the absence of actual thickness profiles. The final third discontinuous ejecta layer, characterized by patchy and noisy pixel intensity in the outer part of the transects, was identified primarily through visual assessment of 2D spatial patterns in images. (Fig. 3E)



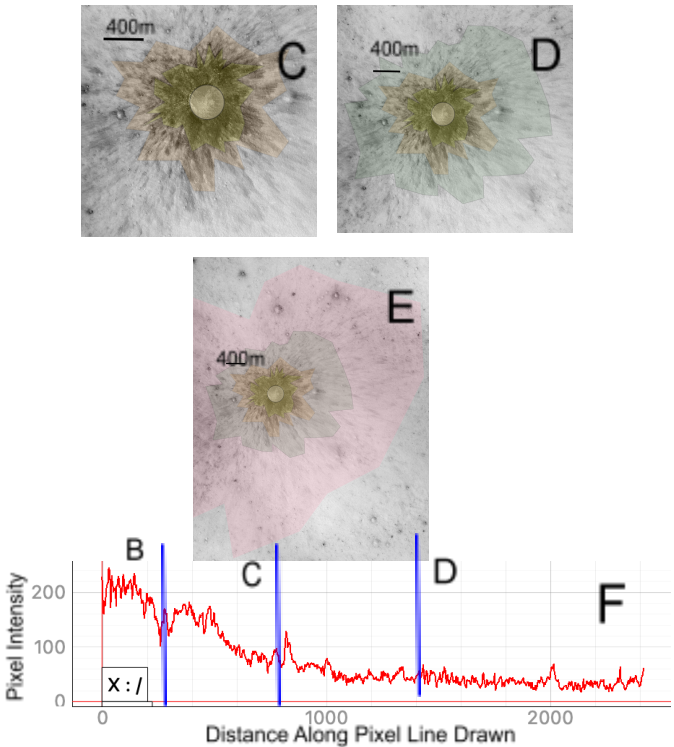


Fig. 3. Ejecta mapping (M1237422334RC) (A) The location of a radial transect (red) is shown in F. (B-E) Continuous and discontinuous ejecta layers. (F) Pixel intensity analysis. Locations of B-D features are highlighted in blue.

We note that radial profiles often showed fewer distinct intensity drops for craters with high rock abundance ($H_{Rock} > 0.05$). In these cases, mapping was simplified to two layers: a continuous ejecta layer and one discontinuous ejecta layer, which we interpret as an equivalent of the third discontinuous ejecta level in remaining objects based on similarities in pixel intensity and overall ejecta morphology.

Preliminary Results: We measured ejecta radii for each level (B-E) by calculating distances between the crater center and points 50 m apart along the polygons' edges. We present the summary of statistics of these measurements for each scaled ejecta layer level (B-E) in Table 1. The table shows the median-scaled ejecta radius ($R_{scaled} = \text{median}(R_{ejecta}/R_{crater})$), the median absolute deviation (MAD), the minimum and maximum R_{scaled} , and the delta (range) in terms of R_{scaled} and the physical distance assuming $R_{cr} = 500\text{m}$ for reference. Ejecta extent increases with the layer level, with medians of 1.487 (continuous ejecta, or B), 2.426 (level C), 3.777 (level D), and 6.506 (level E). Our results reveal that variability expressed as $\Delta R/R_{scaled}$ (1.459–13.199) or MAD in R_{scaled} grows with the ejecta level. Hence, the outermost level is the most sensitive probe of processes that lead to the differences in ejecta deposition and dynamics within that sample.

In Table 2 we report similar statistics, this time for rocky and non-rocky crater ejecta. Non-rocky ejecta extends farther, with broader spreads at higher levels, peaking at 6.875 ± 1.380 (level E). In comparison rocky ejecta are more compact, with smaller radii, peaking at 3.995 ± 1.574 (level E). In those craters, boulders are primarily found in the first two layers, while finer, non-rocky materials dominate the outer layers.

These differences indicate that rock abundance and subsurface material properties strongly influence ejecta radii.

Ejecta Level	Median (R_{scaled})	MAD (R_{scaled})	Min (R_{scaled})	Max (R_{scaled})	DELTA (R_{scaled})	DELTA * 500m
B	1.487	0.178	0.854	2.313	1.459	729.5m
C	2.426	0.418	1.174	4.351	3.177	1588.5m
D	3.777	0.662	1.884	6.84	4.956	2478m
E	6.506	1.907	2.208	15.407	13.199	6599.5m

Table 1: Summary of Scaled Ejecta Radii Statistics for Each Ejecta Layer.

Ejecta Level	Non-Rocky Ejecta (Median (R_{scaled}) \pm MAD)	Rocky Ejecta (Median (R_{scaled}) \pm MAD)
B	1.59 ± 0.197	1.398 ± 0.156
C	2.434 ± 0.339	1.969 ± 0.356
D	3.828 ± 0.484	3.025 ± 3.025
E	6.875 ± 1.380	3.995 ± 1.574

Table 2: Comparison of Scaled Ejecta Radii for Non-Rocky and Rocky Ejecta

Summary: We found that young lunar craters with diameters as large as a few hundred meters are surrounded by ejecta blankets with highly varied scaled ejecta radii (sometimes also referred to in literature as ejecta mobility), i.e. between 2.2–15.4, with median and MAD 6.5 ± 1.9 . Craters excavating consolidated materials have smaller ejecta radii ($R_{scaled} = 4.0 \pm 1.6$), while those impacting loose regoliths produce larger ejecta blankets ($R_{scaled} = 6.9 \pm 1.4$). This suggests a relationship between ejecta radius and rock abundance and further confirms that subsurface properties influence scaled ejecta radii. The physical scale of variations predicted in this study for the outermost edges of ejecta (level E) is significant, as it amounts to multiples of the crater radius. Future work needs to address caveats related to potential variations in surface degradation and reflectance properties of excavated materials between these impact sites.

References: 1. Hörz et al., 1991, Lunar Sourcebook, 61-120, 1991lsug.book...61H 2. Sokolowska et al., 2024, Icarus, 420, 116-150, 10.1016/j.icarus.2024.116150 3. French, 1998, Traces of Catastrophe 4. Melosh, 1989, Impact Cratering 5. Bandfield et al., 2014, Icarus, 231, 221-231, 10.1016/j.icarus.2013.12.017 (2014) 6. Rosas-Chavoya, 2021, Universidad de la Rioja 10.18172/cig.51437. 7. Mouginis-Mark 1979, Journal of Geophysical Research, 84, 10.1029/jb084ib14p08011 8. Chin, 2007, Space Science Reviews, 129(4), 391-419, 10.1007/s11214-007-9153-y 9. Hayne et al., 2017, Geophysical Research, 122, 2371-2400, 10.1002/2017JE005387 10. Williams et al., 2018, Journal of Geophysical Research, 123, 2380-2392, 10.1029/2018JE005652